UCLA
UCLA Previously Published Works

Title
Frequency Tuning of a Disk Resonator Gyro Via Mass Matrix Perturbation

Permalink
https://escholarship.org/uc/item/20j4m9ch

Journal
Journal of Dynamic Systems Measurement and Control, 131(6)

ISSN
0022-0434

Authors
Schwartz, David
Kim, Dong Joon
M'Closkey, Robert T

Publication Date
2009-11-01

DOI
10.1115/1.3155016

Peer reviewed

eScholarship.org Powered by the California Digital Library
University of California

Frequency Tuning of a Disk Resonator Gyro via Mass Matrix Perturbation

David Schwartz*, Dong Joon Kim†, Robert T. M'Closkey ‡

Mechanical and Aerospace Engineering Department

University of California, Los Angeles

Los Angeles, CA 90095 USA. §

June 15, 2009

Abstract

Electrostatic tuning of the resonant modes in microelectromechanical (MEM) vibratory gyroscopes is often suggested as a means for compensating manufacturing aberrations that produce detuned resonances. In high performance sensors, however, this approach places very stringent requirements on the stability of the bias voltages used for tuning. Furthermore, the bias voltage stability must be maintained over the operating environment, especially with regard to temperature variations. An alternative solution to this problem is to use mass perturbations of the sensor's resonant structure for resonant mode tuning. This paper presents a new mass perturbation technique that only relies on the sensor's integrated actuators and pick-offs to guide the mass perturbation process. The algorithm is amenable to automation

*David Schwartz is a Graduate Student Researcher.

†Dong Joon Kim is a Postdoctoral Researcher

‡Robert T. M'Closkey is Professor and corresponding author (rtm@obsidian.seas.ucla.edu, 310 825-2909)

§This work was supported by Boeing, the UC MICRO program, and NSF grant #0601622.

and eliminates the requirement that the modal nodes of the resonator be identified by direct measurement.

1 Introduction

High-performance vibratory angular rate sensors rely on the matching of the frequencies of two modes that are highly coupled by a Coriolis acceleration term when the equations of motion are written in a case-fixed coordinate system. Frequency matching exploits the mechanical gain afforded by the sensor dynamics and leads to the best attainable signal-to-noise ratio. In principle, the degenerate dynamics can be attained by designing structures with a high degree of symmetry such as Litton's Hemispherical Resonator Gyroscope (HRG) [1] and the BAE Silicon Vibrating Structure Gyroscope (SiVSG) [2]. Boeing's Silicon Resonator Gyroscope (SiDRG), shown in Fig. 1, motivates the study in this paper. The results of the paper, however, are relavent for other axisymmetric, planar resonators.[1]

Ideally, the location where the resonant structure attaches to the sensor case is a nodal point for the Coriolis-coupled modes and the symmetric design guarantees degenerate modal frequencies. This scheme isolates the Coriolis-coupled modes from linear base motion and reduces energy dissipation in the modes, thereby eliminating large contributors to angular rate bias and drift. The HRG is an extreme example of the degree of isolation that can be achieved—quality factors exceeding 1×10^6 have been reported when the resonators are fabricated from fused quartz [1].

For those sensors lending themselves to MEM fabrication, such as the SiDRG, local variations in etch rate produce minute, but unpredictable, asymmetries that manifest themselves as a splitting of the modal frequencies (right side of Fig. 1). Although the frequency splits are small, on the order of 0.3% or less, the absolute separation between the modal frequencies coupled with their high quality factors conspire to eliminate the mechanical gain advantage that was a primary objective of the modal degeneracy.

[1] For more information on the operation of vibratory angular rate sensors, refer to [3].

In past work, the resonant frequencies of the SiDRG were tuned by applying electrostatic forces with dedicated electrodes, thereby locally altering the resonator stiffness [4–6]. The drawback of this solution, however, is that the electrodes are required to maintain a voltage stability that is difficult to achieve with compact, low-cost electronics. The possibility of tuning the modes by permanently altering the mass distribution of the resonant structure is attractive because it eliminates the need for electrostatic tuning electronics.

Though no analytical results exist regarding the effects of mass perturbations to the SiDRG's specific structure, results have been documented for a simple ring, which has similar modal characteristics. In an axisymmetric ring, planar modes with the same nodal configuration occur in degenerate pairs which have the same modal frequencies and have indeterminate angular orientations around the axis of symmetry. We will focus on the n=2 Coriolis-coupled modes, which have the elliptical shape illustrated on the left-hand side of Fig. 2, because they are the modes most commonly exploited in axisymmetric vibratory gyroscopes.[2] Studies of rings with small mass and stiffness asymmetries show that the rings have approximately the same elliptical mode shape for the n=2 Coriolis-coupled modes, but that the modes are constrained to two fixed orientations, 45 degrees apart, and at two nearly degenerate modal frequencies (middle of Fig. 2) [8, 9]. Other researchers have derived expressions concerning the effects of mass perturbations on the modal frequencies and the positions of the modal axes and have verified characteristics of these expressions on physical systems [7, 8]. The equations were then used to derive a simple process in which frequency tuning was achieved by adding a point mass to the location of the anti-node of the high frequency mode or by removing a point mass from the location of the anti-node of the low frequency mode (right side of Fig. 2) [9]. This process was verified on a MEM device when laser ablation was employed to remove mass and predictably alter the frequency split [10, 11]. Unfortunately, this process is not easily extended to a "production" environment because the determination of the location of the anti-nodes requires significant effort. The objective of this paper is to develop a tuning algorithm that will use data retrieved from the embedded electrodes as its solitary guide

[2] Much of the analysis, however, applies to higher-order Coriolis-coupled modes as well.

in tuning the modal frequencies.

In order to facilitate the development of the algorithm, a large scale approximate model of the SiDRG, named the Macro DRG, was fabricated for this study (Fig. 3). Although the Macro DRG resonator is not an exact scale replica of the SiDRG resonator, the two share many salient features such as the number of concentric rings and the orientation of the "spokes" connecting them. Our tuning approach is facilitated by a novel model identification method which is applied to multi-input/multi-output empirical frequency response data generated with the Macro DRG. Small magnets are used to effect perturbations to the resonator mass and are modeled as perturbations to the mass matrix identified in the model. The prospect of achieving a tuned state by placing magnets at only one angular location on the resonator is analyzed which motivates the discussion of a more elegant frequency tuning approach. This approach uses only the fixed electromagnetic actuators and fixed capacitive sensors as its guide, successfully circumventing the need to directly identify the location of the anti-node of the higher frequency n=2 mode. In the last section, this approach is successfully demonstrated under several different initial resonator conditions.

2 Macro DRG Experimental Setup

The Macro DRG resonator is machined from cold-rolled steel and has an outer diameter of 11.6 cm (Fig. 3). The resonator thickness is 4.7 mm and each of its nineteen rings is 0.9 mm wide with 1.1 mm gaps between rings. Each ring is connected to its immediate neighbors at eight "spokes," with 45 degrees spacing. The eight spokes connecting a ring to its outer neighbor, however, are rotated by 22.5 degrees from the eight spokes connecting the ring to its inner neighbor. Thus, the positions of the eight spokes alternate radially between positions 22.5 degrees from each other giving sixteen angular spoke locations, as shown. Small NdFeB magnets, disc shape with a 1.6 mm diameter and 0.8 mm thickness, can be attached to the top surface of the resonator to create reversible mass perturbations.

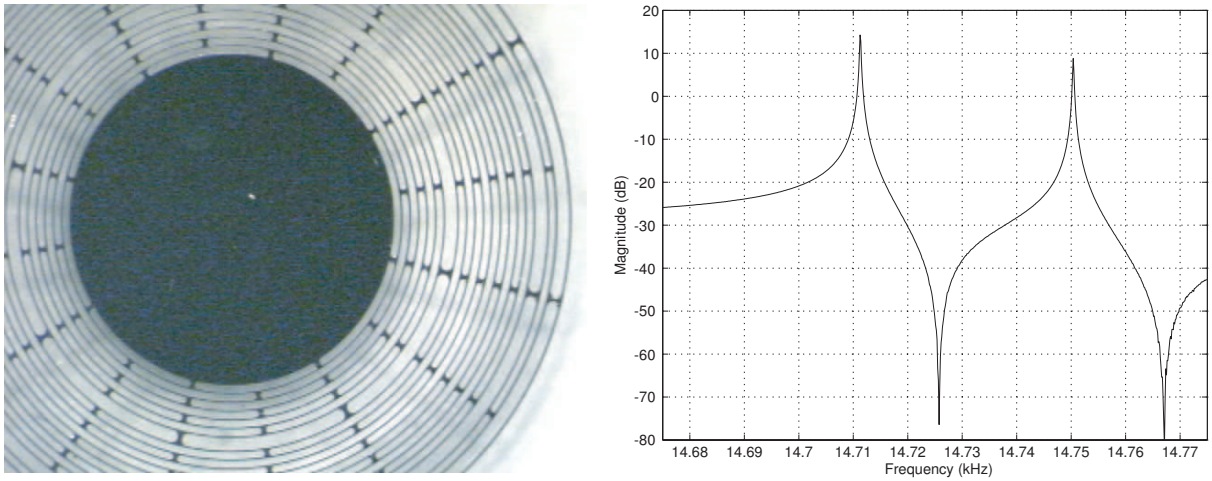

Figure 1: **Left:** Photograph of the resonant structure of the Boeing Silicon Disk Resonator Gyroscope (SiDRG). The n=2 Coriolis-coupled mode of the resonator is generally utilized for rate detection. **Right:** The SiDRG frequency response using embedded drive and sense electrodes within a narrow, 100 Hz band encompassing the "fundamental" Coriolis modes. Though the frequency split is small in a relative sense—less than 0.3%—the sensor effectively has no mechanical gain in this state.

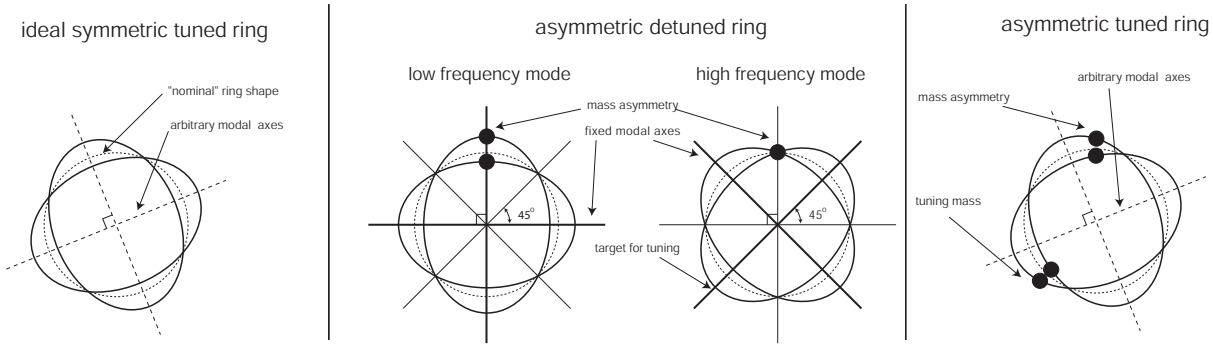

Figure 2: **Left:** Illustration of an n=2 Coriolis-coupled mode in a perfectly axisymmetric ring. This mode appears in a degenerate pair, meaning it can occur with any angular position relative to the axis of symmetry. **Middle:** When slight mass asymmetries exist, the modes manifest themselves in two fixed angular orientations, 45 degrees apart. These modes have two slightly different frequencies and cause the detuning seen in Fig. 1. **Right:** When the correct amount of mass is added to the anti-node of the high frequency mode (the 'target for tuning' on the asymmetric detuned ring), a "tuned" state can be reached. Even though the mass distribution is asymmetric, the important properties of the ideal ring are recovered.

Actuation and sensing of the resonator are achieved using electromagnetic actuators[3] and capacitive sensing pick-offs, each shown in Fig. 3. Each electromagnet is a modified relay, using variable current through its solenoid to exert a radial force on the resonator. Each sensing pick-off consists of a brass disk (5 mm diameter) placed parallel to the outside edge of the outermost ring of the resonator. The resonator is biased at 50 Volts and, as the resonator vibrates, the capacitance between the resonator and the brass disk changes. Charge on the disk flows to the virtual ground of the transimpedance amplifier that is configured with a 1 MΩ resistor, thereby providing a gain of 10^6 V/A. The transimpedance electronics are enclosed in a steel shell to provide partial shielding from the electromagnetic actuators.

The experimental apparatus is shown in Fig. 3. Two electromagnets are placed 45 degrees apart so that they present "orthogonal" excitations with respect to the n=2 Coriolis-coupled modes. The two pick-offs are placed 135 degrees apart in an equally "orthogonal" arrangement.

The block diagram for open loop system identification is shown in Fig. 4. A digital signal processor (DSP) generates band-limited test signals in the desired frequency range. Since the electromagnetic actuator exerts an attractive force for both positive and negative voltages, the desired AC waveform, with a 500 mV maximum amplitude, is biased by 3 Volts. The sense signals are then further amplified ($\times$400), filtered with low-pass eight-pole Butterworth filters possessing 10 kHz cut-off frequencies, and then sampled by the DSP. The drive signals are subjected to the same filter and resampling to account for the filter phase shifts and zero-order hold effects.

The displacement-to-voltage gain on the capacitive pick-offs is extremely sensitive to the width of the air gap between the sensors and the resonator. With this in mind, the actuators and sensors are placed on linear translational stages for precise gap control. The gap calibration setup for the pick-offs, shown as the dotted lines in Fig. 4, involves setting the electromagnet inputs to 0 Volts and the replacing the 50 Volt bias to the resonator with a 1.6 KHz sine wave from a signal generator.

[3]The Macro DRG uses electromagnetic actuation instead of electrostatic actuation because electrostatic forces are too weak for effective actuation at the Macro DRG scale. Furthermore, the gaps required for electrostatic actuation are so small that viscous effects dominate the dynamics of the air in the gaps causing significant nonlinear damping, an effect called squeeze-film damping [13].

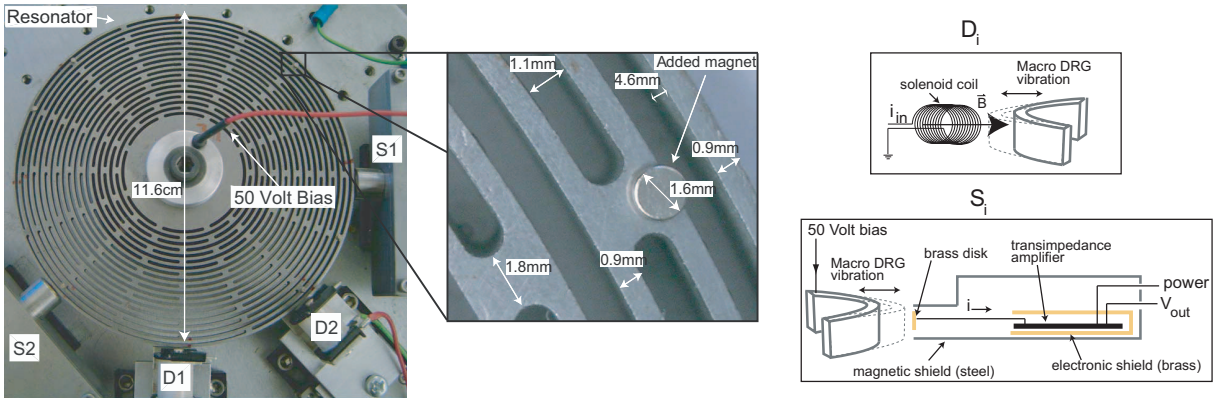

Figure 3: **Left:** Photograph of the Macro DRG. The two electromagnetic actuators are labeled D_1 and D_2, and the two capacitive pick-offs, that detect radial deflection of the resonator, are labeled S_1 and S_2. Small NdFeB magnets are added to create a reversible perturbations of the mass distribution of the resonator. **Top Right:** Diagram of the electromagnetic actuator. **Bottom Right:** Diagram of the capacitive sense pick-off. This design was used to minimize electromagnetic coupling to the transimpedance amplifier.

The responses from the pick-offs are compared to each other and the gaps between the pick-offs and the resonator are adjusted until the responses exhibit the same amplitude. This process ensures that the pick-offs will have the same gain at frequencies near those of the fundamental Coriolis-coupled modes. The electromagnets are much harder to calibrate, but the same level of precision is not required due to the nature of the force created by the magnetic flux. The gap is set to 1 mm, which is large enough to have a minimal detrimental effect on the quality factor of the resonator while still achieving an adequately large excitation force.

A single channel of Macro DRG frequency response data is shown in Fig. 5. The fundamental Coriolis modes are near 1.6 kHz and appear as one resonant peak at this scale. The zoomed frequency responses, shown at the right, display the individual Coriolis-coupled modes with approximately a 1.6 Hz (0.1%) frequency split. This two-input/two-output empirical frequency response format will be used as the principal guide to the model fitting and tuning algorithms.

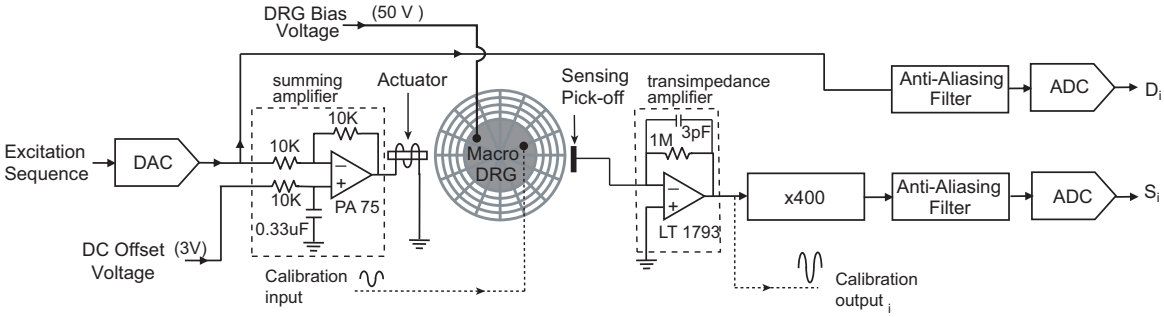

Figure 4: Block diagram of test setup. The filtered drive and sense signals are denoted D_i and S_i, $i = 1, 2$, respectively. Frequency response data is used to construct a two-input/two-output model of the Macro DRG dynamics. The dotted path represents an alternative setup that is used to calibrate gaps between the pick-offs and the resonator.

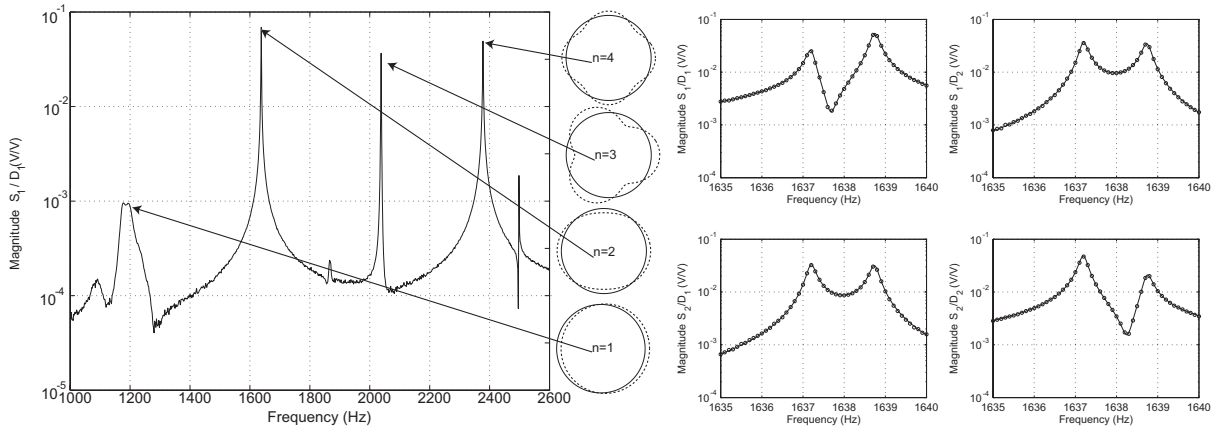

Figure 5: **Left:** The S_1/D_1 channel of the empirical wideband frequency response of the Macro DRG showing several resonator modes. At this scale there appears to be no split between the n=2 modes (near 1.6 kHz). **Right:** The narrowband dynamics of all four channels in a neighborhood of the fundamental Coriolis-coupled modes. The data points are represented by '○' while the trace through the points is a model that was fit using the process described later in this paper. Just as in the SiDRG response, the Coriolis-coupled modes of the Macro DRG have a small frequency split despite the fact that the steel resonator is highly symmetric.

3 Sensor Model

3.1 Model Development

The system identification method for guiding the mass perturbation process is based on the one developed by the authors for electrostatic tuning of the gyro dynamics [6] . For mass tuning, the linear mechanics of nearly degenerate vibratory gyros in a neighborhood of the Coriolis-coupled modes can be modeled as

$$H_{out}(s)RZ_{act(k)}^{-1}(s), \tag{1}$$

where s is the Laplace transform variable and where

$$Z_{act(k)}(s) := (M_0 + \Delta_k)s^2 + Cs + K. \tag{2}$$

In this model, C and K are real 2×2 positive definite damping and stiffness matrices, M_0 is the real 2×2 positive definite nominal mass matrix, and Δ_k is the perturbation to M_0 due to the particular arrangement of added magnets in the kth perturbation case. The angular rotation rate of the sensor is assumed to be zero in this model. The subscript on Z_{act} denotes that the system matrices are written in the generalized coordinates specified by the actuator (forcer) frame. The transfer function H_{out} represents any dynamics associated with the signal conditioning electronics and $R \in \mathbf{R}^{2\times 2}$ captures the effects of non-colocated pick-offs and forcers.

The model parameters $\{M_0, \Delta_1, \Delta_2, \ldots, \Delta_{n_p}, C, K, H_{out}R\}$ are estimated by fitting frequency response data from $n_p + 1$ experiments conducted with different mass perturbation scenarios to (1). In other words, the kth experiment yields two-input/two-output complex valued frequency response data $\{\psi_{k,1}, \psi_{k,2}, \ldots, \psi_{k,m_k}\}$ corresponding to the m_k real frequencies $\{\omega_{k,1}, \omega_{k,2}, \ldots, \omega_{k,m_k}\}$.

The minimax optimization problem for estimating the sensor parameters is

$$\min_{\substack{M_0+\Delta_p>0 \\ K>0, C>0, M_0>I \\ R_l \in \mathbf{C}^{2\times 2},\, l=0,1,\ldots,n_R}} \; \max_{\substack{k=0,\ldots,n_p \\ q=1,\ldots,m_k}} \overline{\sigma}\left(\tilde{R}_{k,q} - \psi_{k,q} Z_{act(k)}(j\omega_{k,q})\right), \tag{3}$$

where

$$\tilde{R}_{k,q} := \sum_{l=0}^{n_R} R_l \omega_{k,q}^l, \tag{4}$$

and where evaluating Z_{act} at the qth frequency point associated with the kth experiment yields

$$Z_{act(k)}(j\omega_{k,q}) := -(M_0 + \Delta_k)\,\omega_{k,q}^2 + K + jC\omega_{k,q}. \tag{5}$$

The constraint $M_0 > I$ in (3) is imposed rather than the typical $M_0 > 0$ because in the latter case all of the free parameters may be scaled by a nonzero constant so as to make the cost arbitrarily small without actually changing the model frequency response. Also note that $H_{\text{out}}R$ has been replaced by $\tilde{R}$. This recognizes the fact that any additional dynamics due to, for example, signal conditioning preamplifiers, should not exhibit significant magnitude and phase changes in a neighborhood of the resonant modes. If these dynamics can be reflected to the sensor output then they can be combined with R into a low order polynomial function of frequency with coefficients in $\mathbf{C}^{2\times 2}$, i.e. $\tilde{R}$ is degree n_R. In fact, $\tilde{R}$ can be viewed as the combination of the first few terms of the Taylor series expansion of the frequency response function of H_{out} including the non-collocation effects. Finally, $\overline{\sigma}$ denotes the largest singular value. Thus (3) is a multi-input/multi-output extension of the first iteration of the Sanathanan-Koerner frequency domain model fitting algorithm [14]. Note that (3) can be restated as following eigenvalue problem

$$\begin{array}{ll} \text{min:} & \gamma \\ \text{subject to:} & J_{qk} > 0,\, q = 1,\ldots,m, k = 0,\ldots,n_p \\ & M_0 > I,\, (M_0 + \Delta_k) > 0,\, C > 0,\, K > 0 \\ & \Delta_0 = 0, R_l \in \mathbf{C}^{2\times 2},\, l = 0,\ldots,n_R \end{array}, \tag{6}$$

where

$$J_{qk} := \begin{bmatrix} \gamma I & \left(\tilde{R}_q - \psi_{k,q} Z_{\text{act(k)}}(j\omega_q)\right)^* \\ \tilde{R}_q - \psi_{k,q} Z_{\text{act(k)}}(j\omega_q) & \gamma I \end{bmatrix}.$$

This problem can efficiently be solved using a number of commercially available packages.

3.2 Verification of the Model

As in Fig. 5, experimental data are generated by driving each actuator with a chirp sequence whose 5 Hz bandwidth encompasses the fundamental Coriolis modes of the Macro DRG. The input-

output sequences are processed to yield 2×2 empirical frequency response data on a grid of frequencies with 0.1 Hz resolution giving fifty-one frequency response points in each plot. The model (2) is applied to two mass perturbation cases in addition to the nominal case in which no mass perturbation is present. The first mass perturbation case places four magnets on outer ring of the Macro DRG, as shown in the left-hand illustration of Fig. 6, and is represented by the Δ_1 mass matrix perturbation. The four-fold symmetry of the mode shape guarantees that this perturbation will have the same effect as adding the four masses to only one of these four positions. The second mass perturbation case places four magnets on the outer ring of the DRG, as shown in the right-hand illustration of Fig. 6, and is represented by the Δ_2 perturbation. The empirical frequency responses for these perturbed cases along with the case in which no magnets are added are shown in Figs. 7 and 8. Since the sensor is a two-input/two-output plant, the four magnitude plots are shown in Fig. 7 and the four phase plots are shown in Fig. 8 (the individual channels are denoted S_1/D_1, S_2/D_1, etc.). It is clear that the mass perturbations cause a shift in the modal frequencies and alter the split between these frequencies. The model parameter set $\{M_0, \Delta_1, \Delta_2, C, K, R_0, R_1\}$ is determined from (6). The model frequency responses are given by $(R_0 + j\omega R_1)\left(-(M_0 + \Delta_k)\,\omega^2 + K + jC\omega\right)^{-1}$, k = 0,1,2, and are plotted as the solid traces in Figs. 7 and 8. Note, the order of $\tilde{R}$, n_R, is set to 2 for this and future models. The model fit is almost indistinguishable from the empirical data—the largest deviation is only 5%.

Since we are interested in using this model to guide the mass addition/removal process with the objective of driving the two modal frequencies together, its predictive power is of great importance and is tested in two ways. In the first test, two magnets are added to each of the four points on the resonator corresponding to the positions shown in the left-hand illustration in Fig. 6 (total of eight magnets). This perturbation doubles the magnitude of the mass perturbation corresponding to Δ_1 so we compare the empirical data with the frequency response of the model

$$(R_0 + j\omega R_1)\left(-(M_0 + 2\Delta_1)\omega^2 + K + j\omega C\right)^{-1}.$$

The comparison is made in Fig. 9. The model predicts the empirical frequency response data extremely well.

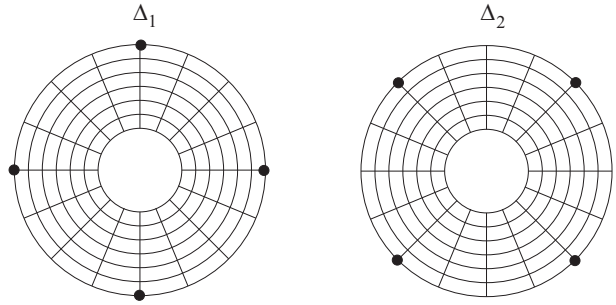

Figure 6: **Left:** Orientation of Δ_1 perturbation. **Right:** Orientation of Δ_2 perturbation. Masses are added at four points in each case to achieve the most even possible mass loading. These are the perturbations corresponding to '$\square$' and '$\diamondsuit$' in Figs. 7 and 8.

The second test case involves placing a single magnet at each of the eight points on the resonator corresponding to the locations shown in both illustrations in Fig. 6. This perturbation should correspond to modifying the nominal mass matrix by the sum of Δ_1 and Δ_2. Thus we compare the frequency response data against the model

$$(R_0 + j\omega R_1)\left(-(M_0 + \Delta_1 + \Delta_2)\omega^2 + K + j\omega C\right)^{-1}.$$

Again, the set of plots in Fig. 10 shows very good agreement between the model prediction and the empirical frequency response data. This verifies the predictive power of the model fitting technique and the assumption that the addition of the magnets can be modeled purely as a mass matrix perturbation.

4 Tuning the Modal Frequencies

4.1 Frequency Tuning by Perturbing One Unique Circumferential Location

Now that the experimental setup and modeling techniques are identified, we begin to develop potential processes for driving the modal frequencies of the Macro DRG together and reaching a 'tuned' state. It is clear from Fig. 7 that the angular location of a mass perturbation affects the

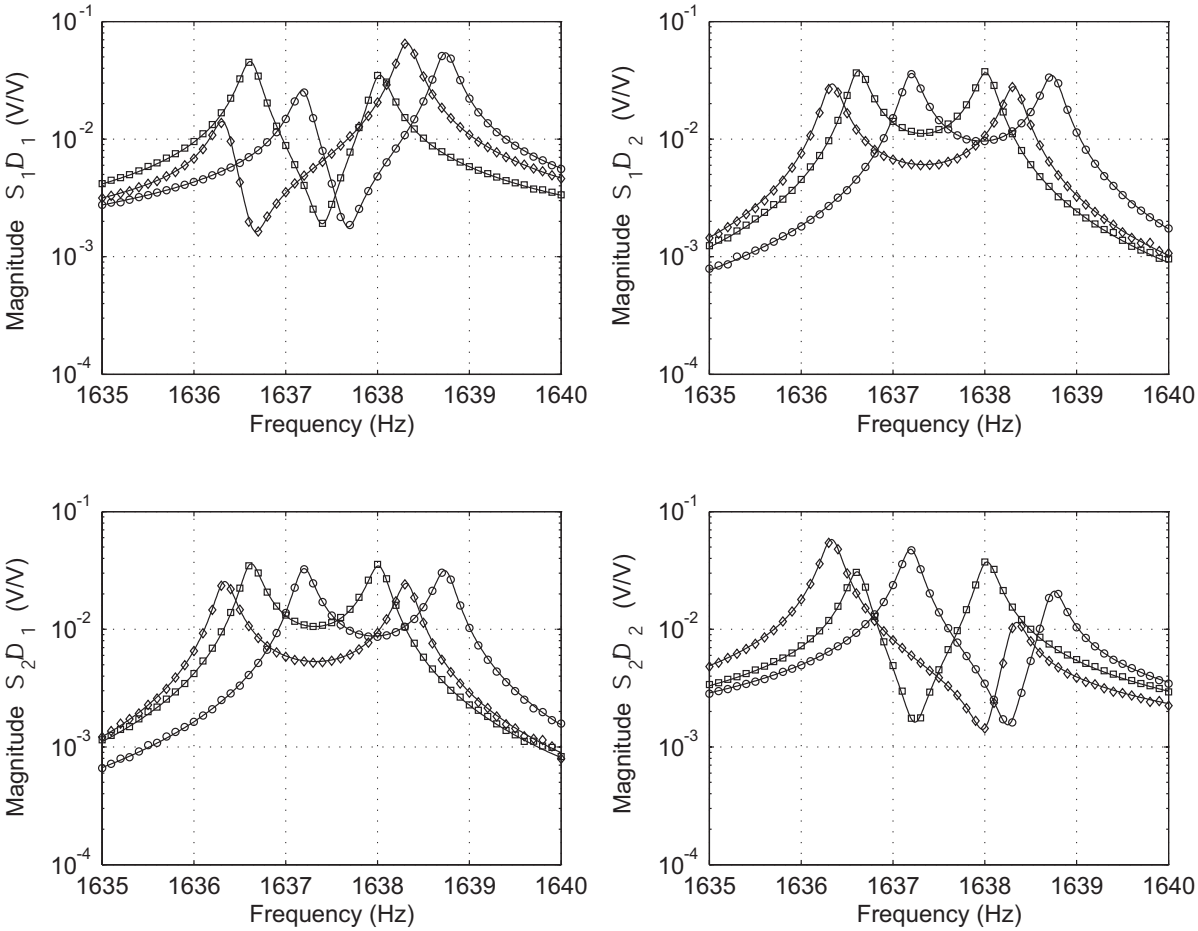

Figure 7: The two-input/two-output empirical and model frequency response magnitudes used to test the model fitting algorithm. The empirical data for the test with no perturbation is represented by '$\circ$' and the data resulting from the Δ_1 and Δ_2 perturbations (shown in Fig. 6) are represented by '$\square$' and '$\diamondsuit$' respectively. The model fits given by $(R_0 + j\omega R_1)(-(M_0 + \Delta_k)\omega^2 + K + j\omega C)^{-1}$ of the three data sets are the solid traces. Thus, the change in the frequency response due to the addition of magnets is successfully modeled as a change to only the mass matrix.

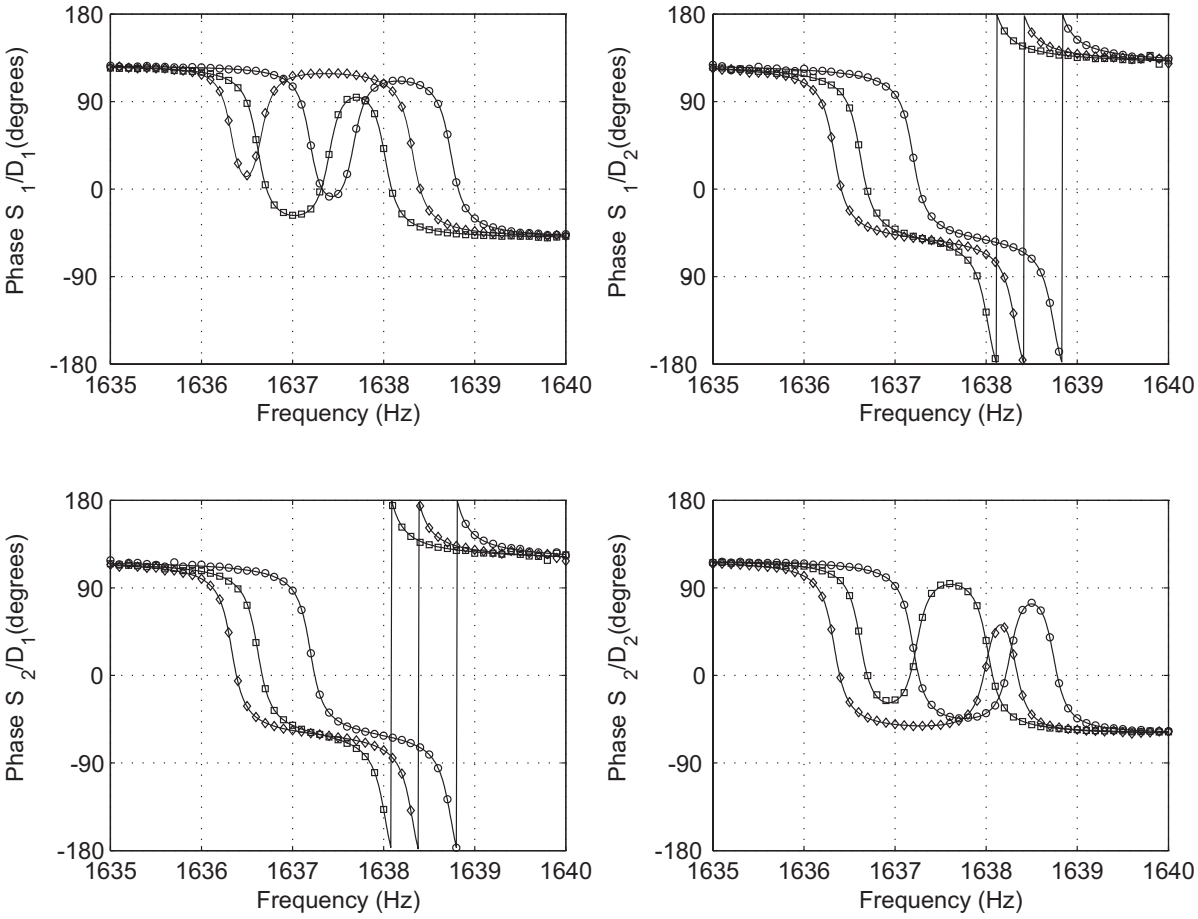

Figure 8: The two-input/two-output empirical and model frequency response phase plots corresponding to the magnitude plots in Fig. 7.

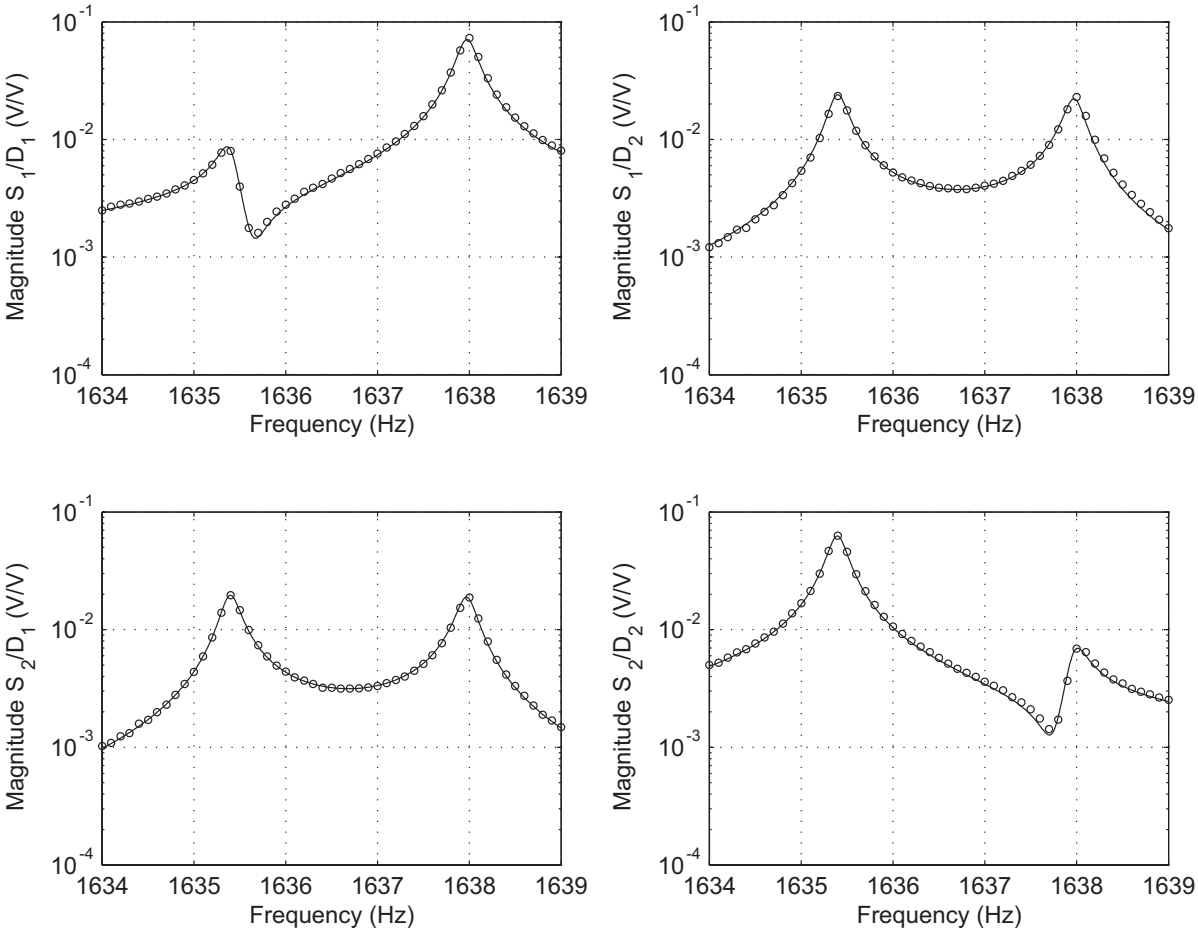

Figure 9: Empirical frequency response of Macro DRG with double the mass perturbation at the Δ_1 perturbation locations ('$\circ$') compared to the frequency response predicted by the model $(R_0 + j\omega R_1)\,(-(M_0 + 2\Delta_1)\omega^2 + K + j\omega C)^{-1}$ (solid trace).

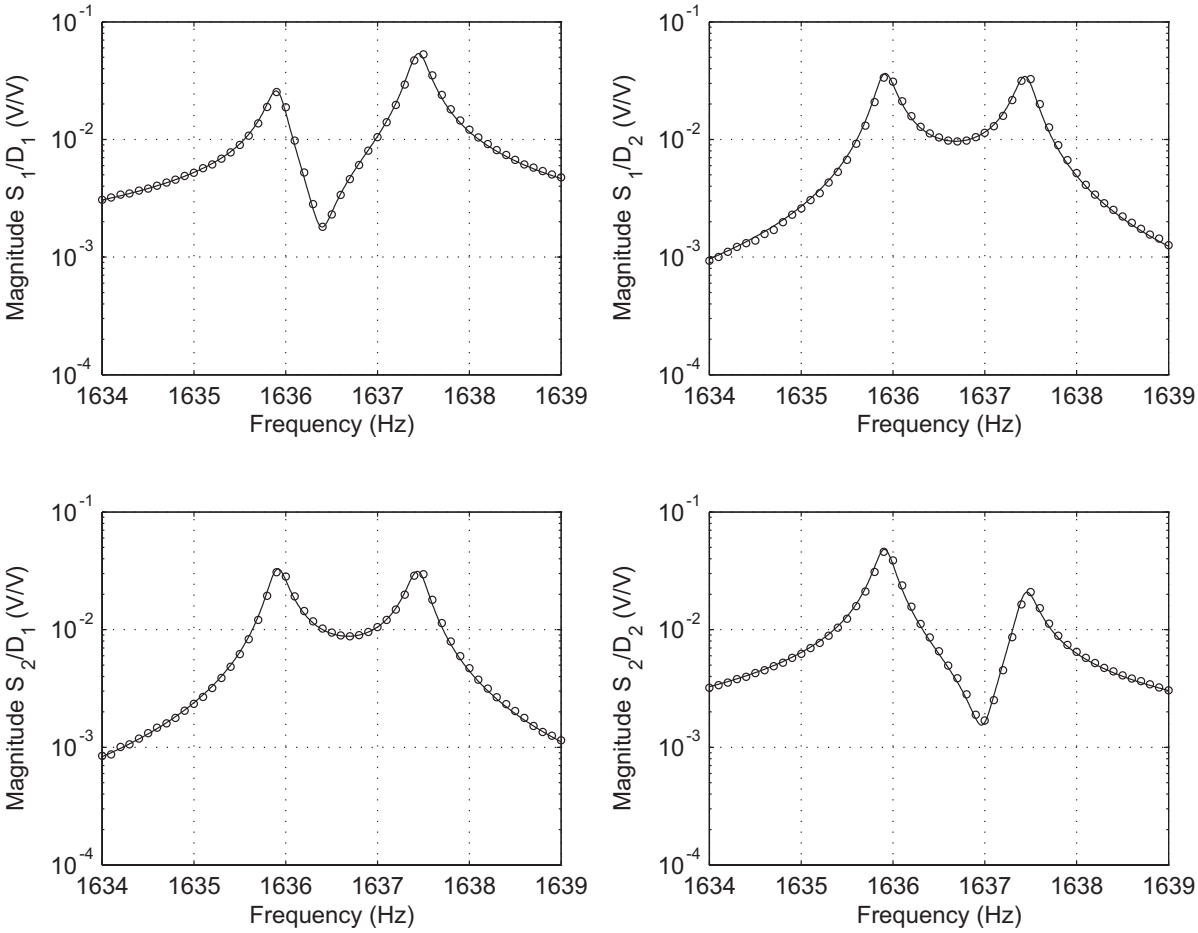

Figure 10: Empirical frequency response of Macro DRG with the mass perturbations in both the Δ_1 and Δ_2 perturbation locations ('$\circ$') compared to the frequency response predicted by the model $(R_0 + j\omega R_1)\,(-(M_0 + \Delta_1 + \Delta_2)\omega^2 + K + j\omega C)^{-1}$ (solid trace).

resulting frequency split. For a simple ring, frequency tuning can be achieved by adding mass to only one location—the anti-node of the high frequency mode (Fig. 2) [9]. In many ways this is the simplest solution to the general frequency tuning problem and in this section we test this methodology as applied to the Macro DRG using several different techniques. The lessons learned from this exercise motivate the development of a tuning process that is better suited for axisymmetric vibratory gyroscopes. Our first step is the direct measurement of the mode shape of the detuned Macro DRG.

4.1.1 Measuring the mode shape

In this experiment, the radial motion of the outer ring is measured by a laser vibrometer. One of the electromagnets is used to excite the Macro DRG at the modal frequency corresponding to the higher of the two n=2 Coriolis-coupled mode frequencies. The previous testing setup is placed on a rotational stage while the laser vibrometer is in a fixed position (Fig. 11). Vibration measurements were taken every 2 degrees on a 90 degree arc. The resulting mode shape is shown as the right-hand plot of Fig. 11, with the peak displacement occurring at 77 degrees. It is important to note that the mode shape follows a sine wave fairly well, but not perfectly, making it difficult to utilize a sine wave model to predict the location of the anti-node of the high frequency mode. This experiment essentially replicates the procedure for identifying a mass tuning location suggested for simple rings and provides some interesting information, but does not satisfy the stated goal of using only the fixed electromagnetic drivers and capacitive sensors to guide the tuning.

4.1.2 Testing frequency tuning near the anti-node

The first tuning attempt places multiple magnets at 76 degrees from the D_1 axes and subsequently measures the resulting frequency responses. The resonant frequencies from these responses are calculated by taking the square roots of $\overline{\lambda}_{M,K}$ and $\underline{\lambda}_{M,K}$, the larger and smaller generalized eigenvalues, respectively, of the identified mass and stiffness matrices. The split between these frequencies is plotted in the right-hand graph of Fig. 12. As the first several magnets are added, the split

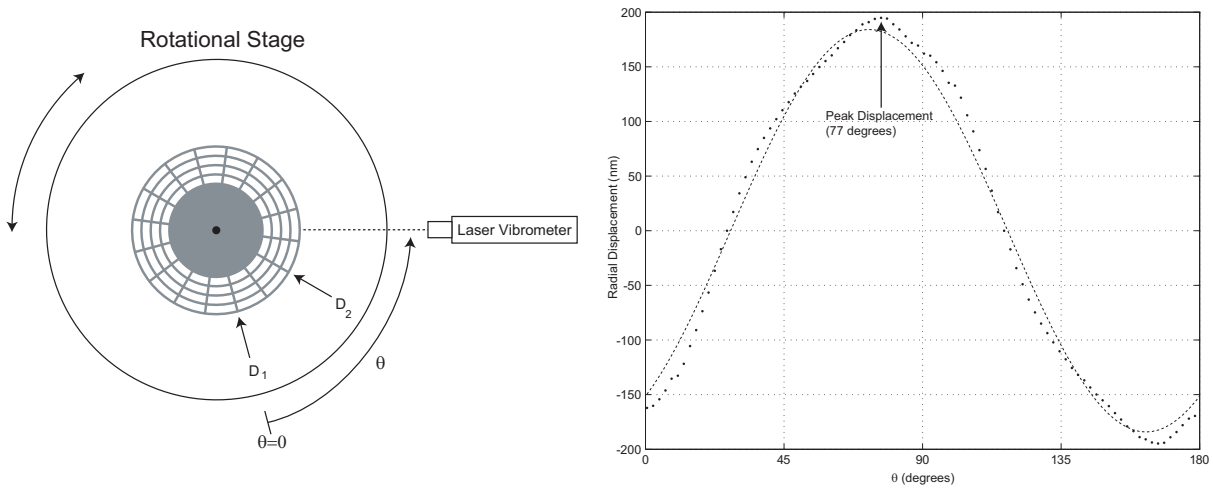

Figure 11: **Left:** Illustration of the testing setup used to determine the radial deflection of the outermost ring of the Macro DRG resonator. The driving electromagnet and the resonator are fixed on the rotational stage so that the deflection can be measured at 2 degree increments. **Right:** Plot of the radial deflection as a function of angular position. The dots represent the experimental data, while the dotted line is a sine wave fit. The large deviations from the sine wave are most likely caused by the additional stiffness provided by the spokes. One proposed tuning method involves adding mass directly to the resonator at the location corresponding to the anti-node of the experimental data. This is the method that has been used in the past to tune other ring shaped devices.

decreases. Before an adequately small split is reached, however, further addition of magnets increases the split. This practice was repeated at 72, 74, 78 and 80 degrees from the D_1 axes and the data are plotted on the left-hand side of Fig. 12. Though the plots are faceted due to the discrete amount of mass added with each magnet, it still appears from Fig. 12 that the best tuning location is approximately 77 degrees from the D_1 axes. It should be noted, however, that misplacing magnets by only 3 degrees increases the minimum achieved split from about 0.15 Hz to 0.4 Hz. This behavior closely follows the mass perturbation model derived in [9] for a simple ring and is simple to explain. To wit, when mass is placed directly at the anti-node of the high frequency mode, the frequency split is reduced, and the anti-node remains in the same location until the split is eliminated. If more mass is added after the split reaches zero, the locale where mass is added becomes the new low frequency anti-node and the split begins to increase. If the initial magnet is misplaced, however, the high frequency anti-node shifts away from the locale of the added magnet. Though at first the split decreases, the split begins to increase when the added magnet is closer to the low frequency anti-node than it is to the high frequency anti-node. Thus, as the error in the location choice increases, the frequency split increases with fewer added magnets, thereby increasing the minimum achievable split when attempting to tune by adding mass to one unique angular location.

The solid trace on the right-hand side of Fig. 12 is an attempt to simulate the minimum achievable split if mass could be added continuously when tuning 76 degrees from the D_1 axes. The Δ associated with the first four magnets added was found using a model fit to the empirical frequency response data of the case with no magnets added and the case with four magnets added at 76 degrees. Next, the split was predicted using the frequencies derived from $\overline{\lambda}_{M_0+\frac{\alpha}{4}\Delta,K}$ and $\underline{\lambda}_{M_0+\frac{\alpha}{4}\Delta,K}$, where α is the number magnets added. The plot demonstrates that the model fitting process proves helpful in determining the minimal split associated with a particular mass perturbation. This realization inspires the proposed tuning method described in the following subsection.

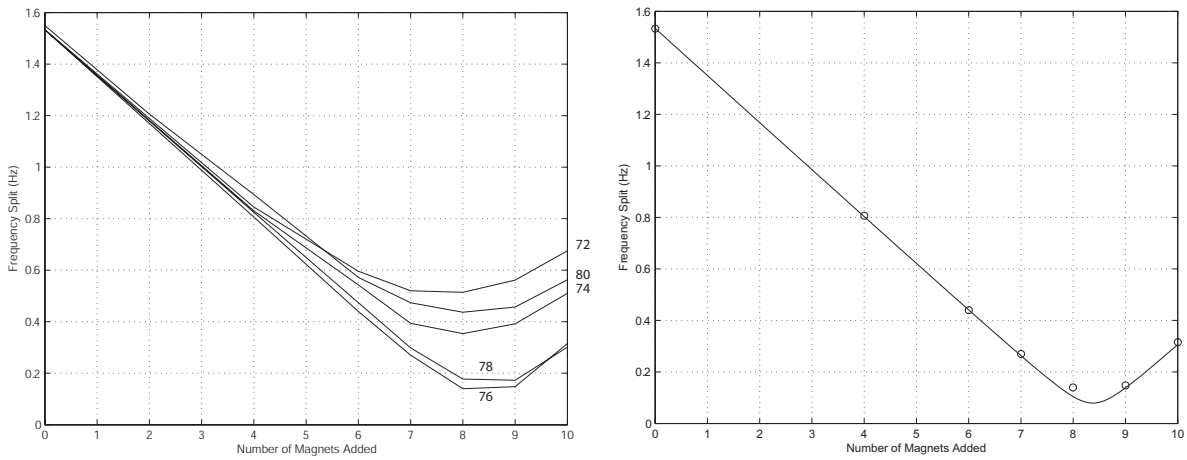

Figure 12: **Left:** The five traces represent five experimental attempts to tune the Macro DRG by placing magnets at only one angular location, using locations of 72, 74, 76, 78 and 80 degrees. Data was taken when 0, 4, 6, 7, 8, 9 and 10 magnets were added for each case. The frequency splits are determined from the models that are fit to the individual experimentally determined frequency responses. In each case the split is at first reduced but at some point further addition of mass increases the split. It appears that the smallest split would be achieved near a location of 77 degrees. It is interesting to note that if the placement is as little as 3 degrees away from this location, the minimum split increases to nearly 0.4 Hz. **Right:** The data taken when tuning is attempted at 76 degrees is replicated as '$\circ$' in this plot. The solid line fit is done by fitting the empirical data from the first two points to a set $\{M_0, \Delta, C, K, R_0, R_1\}$ and using $\overline{\lambda}_{M_0+\frac{\alpha}{4}\Delta,K}$ and $\underline{\lambda}_{M_0+\frac{\alpha}{4}\Delta,K}$ to determine the split for any number of magnets (where α is the number of masses added). This is a good test of the predictive relevance of the model, but also shows how much the minimum achievable split is increased by using a quantized amount of mass.

4.1.3 Δ as a function of angular position on the outer ring

The function $\overline{\Delta}(\theta)$ is defined as the relationship between $\overline{\Delta}$, the mass matrix perturbation associated with one magnet placed upon the outermost ring, and θ, the angular position of that additional magnet. Once the function $\overline{\Delta}(\theta)$ is known, an angle, $\tilde{\theta}$, and an "intensity",α, representing the number of magnets, can be found such that $\overline{\lambda}_{M_0+\alpha\overline{\Delta}(\tilde{\theta}),K} = \underline{\lambda}_{M_0+\alpha\overline{\Delta}(\tilde{\theta}),K}$, implying that the frequency split is eliminated. An experiment is performed to find $\overline{\Delta}(\theta)$ for values of θ in one 90 degree arc.[4] Eight separate perturbations were conducted with magnets spaced in 11.25 degree steps (a total of nine MIMO frequency response data sets) and then the model parameter set $\{M_0, \Delta_1, \ldots, \Delta_8, C, K, R_0, R_1\}$ was identified. Plots of the upper diagonal, lower diagonal and off diagonal terms of each Δ_k, $k = 1, 2, \ldots, 8$, are shown in Fig. 13. Linear interpolation can be used to approximate $\overline{\Delta}$ for any θ. When $\tilde{\theta} = 75.4$ degrees and $\alpha = 8.4$ magnets, $\overline{\lambda}_{M_0+\alpha\overline{\Delta}(\tilde{\theta}),K} = \underline{\lambda}_{M_0+\alpha\overline{\Delta}(\tilde{\theta}),K}$ so the modes are tuned according to the model. According to Fig. 12, though, the minimal split would be about 0.2 Hz if tuning were attempted at only this location. Unfortunately, it is not practical to use the experimental relationship of Fig. 13 on a different Macro DRG. Any small difference in the drive and sense gap distances or in the internal stiffness and damping changes $\overline{\Delta}(\theta)$ significantly enough to reduce its predictive value. Thus, to use this approach, this entire experiment would have to be repeated for every new device, requiring excessive, and likely unnecessary, perturbations.

4.1.4 The eigenvectors of M and K

The next method we analyze uses the generalized eigenvector associated with $\overline{\lambda}_{M,K}$ to identify the location of the high-frequency anti-node. The physical interpretation of the generalized eigenvector relies on the coordinate system of the equations of motion. Because the equations of motion are written in the actuators' reference frame (refer to (1)), the ratio of the two elements of a generalized

[4] It can be shown that adding the same mass at 90, or 180, degree angles relative to the current position produces the same mass matrix perturbation for the modes of interest. Thus, the experimental results for the first 90 degree arc can be extrapolated to represent perturbations to any angular location on the structure.

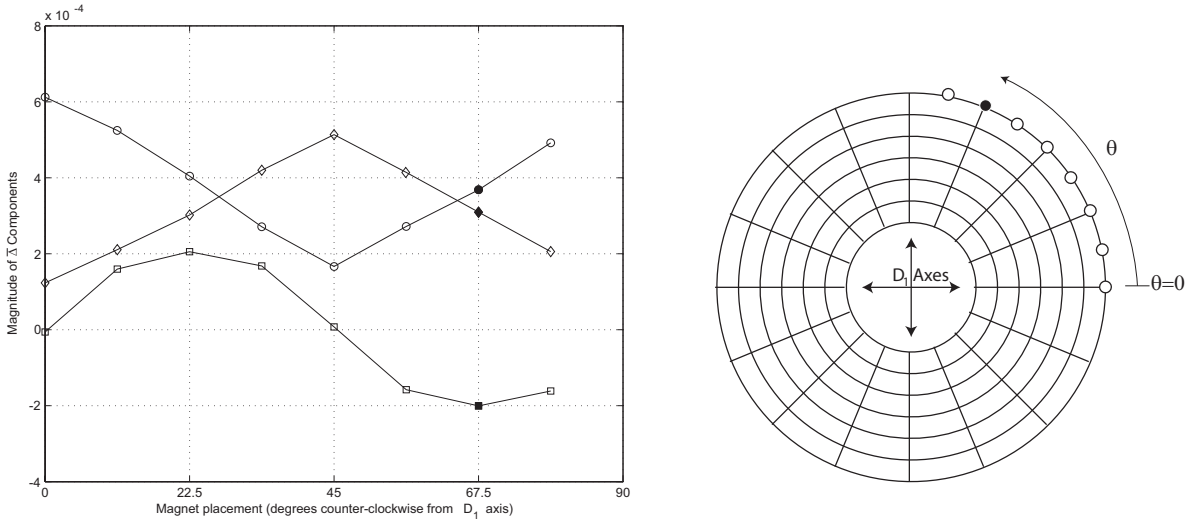

Figure 13: **Left:** Mass matrix perturbation, $\overline{\Delta}$, as a function of the counter-clockwise angle from the D_1 axes, θ, found by fitting the model to nine empirical frequency response data sets. The upper diagonal term is denoted by '$\diamondsuit$', the lower diagonal by '$\circ$', and the off diagonal term by '$\square$'. **Right:** Illustration of the eight placements of the magnet in the tests. When the experiment is repeated with different gap widths for the actuators and sensors, and different initial magnet distributions, the functional relationship varied only slightly. The absolute magnitudes are not important because the model parameter set is scaled by the $M_0 > I$ constraint in (6). The relative magnitudes, however, are at the very least interesting. The solid black magnet in the right hand picture illustrates the perturbation that corresponds to the data points that are solid black in the left-hand figure.

eigenvector is a measurement of the ratio of the amplitudes of the radial velocity of the Macro DRG at the two actuator locations when the DRG is excited at the eigenvector's corresponding eigen-frequency. In order to use this information to estimate the mode shape, the amplitude of the radial motion, u, is approximated by $u = Acos\left(2\left(\theta - \Phi\right)\right)$ where A is the maximum amplitude of the displacement and θ is the angular location as measured from the D_1 axes (Fig. 14). This is an approximation of the true shape given in Fig. 11. The amplitude of motion at the first and second actuators would be $Acos(2\Phi)$ and $Asin(2\Phi)$ respectively. Thus Φ, the angular location of anti-node of the high frequency mode, can be approximated by

$$\Phi = \tfrac{1}{2} tan^{-1}\left(\frac{v_1}{v_2}\right), \tag{7}$$

where v_1 and v_2 are the first and second elements, respectively, of the eigenvector associated with $\overline{\lambda}_{M,K}$. In the case of the unperturbed Macro DRG we find $\Phi = 75$ degrees. This method is particularly attractive because it does not require any experimentation besides the initial frequency response test to approximate the location of the anti-nodes. It appears to be slightly less accurate than the estimate found by directly using $\overline{\Delta}$ and would result in a minimal split of approximately 0.3 Hz if tuning were attempted at only this predicted location.

This method can be improved if one abandons the notion of using only one angular location for tuning. In this improvement, after each magnet is added and a new empirical frequency response is performed, a new model parameter set is found with a new anti-node location. This new location is the target for the next added magnet. Essentially, the effect of the estimate error is negated by "chasing" the location of the high frequency anti-node around the resonator. This method proves successful, guaranteeing a final frequency split of less than 0.1 Hz, but lacks elegance and would be difficult to practice on the SiDRG. A more elegant method is presented in the next section in which the anti-node is essentially "trapped" between two spokes on which tuning masses are added.

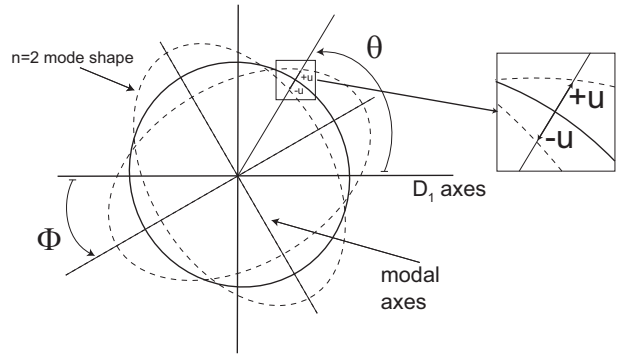

Figure 14: Illustration of the assumed mode shape of the ring using $u = Acos\left(2\left(\theta - \Phi\right)\right)$, where Φ indicates the location of the anti-nodes of the mode shape, and u is the radial displacement of the mode shape as a function of the angle θ. We will use this notation to approximate the mode shape of the n=2 Coriolis-coupled mode of the Macro DRG.

4.2 Frequency Tuning Using Mass Perturbation at the Spokes

When the tuning problem is generalized to allow two tuning locations the solution is much more robust to errors in magnet placement. By choosing mass loading locations on either side of the anti-node of the high frequency mode, the anti-nodal orientation is, in a sense, trapped. For a MEM structure such as the SiDRG, it is easiest to add mass at the spokes of the resonator (visible in Fig. 3 as the structures that join adjacent rings and form a radial pattern) that are closest to the anti-node. In this scenario the perturbed mass matrix is given by

$$M(\alpha_1, \alpha_2) = M_0 + \alpha_1 \Delta_1 + \alpha_2 \Delta_2, \tag{8}$$

where Δ_1 and Δ_2 correspond to the mass matrix perturbations associated with the addition of mass to the two tuning spokes. The number of magnets added to the two spokes for tuning, α_1 and α_2, can be calculated by solving the generalized eigenvalue problem

$$\begin{array}{ll} \text{min:} & \lambda_1 - \lambda_2 \\ \text{subject to:} & \lambda_i > 0,\ i = 1,2 \\ & \lambda_1 M(\alpha_1, \alpha_2) - K > 0 \\ & \lambda_2 M(\alpha_1, \alpha_2) - K < 0 \end{array} . \tag{9}$$

This optimization simultaneously forces λ_1 and λ_2 to become the largest and smallest generalized eigenvalues of M and K and varies α_1 and α_2 to minimize $\lambda_1 - \lambda_2$. If the spokes are chosen correctly, the final cost will be zero and the resulting α_1 and α_2 will create degenerate modal frequencies. Again this optimization can be efficiently solved with a number of commercially available packages.

The entire tuning process can be outlined in a three step algorithm. First, we start with the data for the unperturbed Macro DRG (represented by '$\circ$' in Fig. 16). In the first step, a model is fit to this data set and Φ is approximated as 79 degrees using (7). The approximation implies that anti-node of the high frequency mode falls between the two spokes labeled 4 and 1 in the left-hand illustration in Fig. 15. Thus these spokes are chosen as the targets for tuning. The second step acts as a calibration step for the mass matrix perturbations Δ_1 and Δ_2. Two magnets are added to spoke 4 to represent the Δ_1 perturbation and an empirical frequency response is measured. Then, two magnets are added to spoke 1 and a third frequency response is measured. Using the three frequency response sets, the model parameters $\{M_0, \Delta_1, \Delta_2, C, K, R_0, R_1\}$ are identified. Figure 16 shows the three empirical frequency response sets measured during the first two steps. As expected, with each added magnet the resonant frequencies and their relative split are reduced. In the third step the number of magnets that need to be added to each spoke, α_1 and α_2, are calculated from (9).

This optimization is solved with $\alpha_1 = 7.2$ and $\alpha_2 = 3.2$, rendering the system with M as in (8) degenerate. We can only add quantized amounts of mass onto the rings, so 3 masses are added to spoke 1, and 7 to spoke 4, as shown in the right-hand illustration of Fig. 15. The final empirical frequency response is acquired and is shown in Fig. 17. Note that the response in the off diagonal channels are significantly reduced, which is a positive indication of a nearly degenerate resonator. After model identification is performed on this last data set, the split is found to be only 0.08 Hz, and for all practical purposes the sensor is tuned.

The algorithm was then applied to an array of initial mass distributions. For these tests, a larger magnet (diameter 3.2mm) is placed on the outside surface of the outermost ring at positions

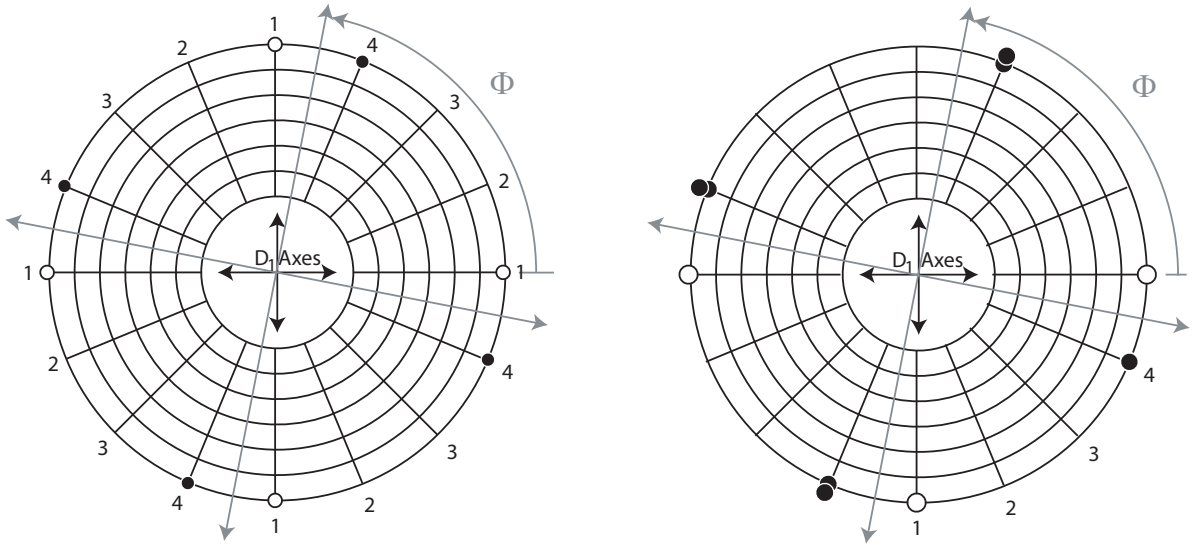

Figure 15: **Left:** Illustration of the identified spokes for mass loading for the example in the text. The gray axes represent the approximated anti-nodal axes of the unperturbed Macro DRG. The small white circles represent where the two magnets may be placed to calibrate the spoke 1, and the two black circles represent where two more may be added to calibrate spoke 4. **Right:** The final orientation of the magnets that successfully tunes the Macro DRG so that the anti-nodal axes are "trapped" between the tuning spokes. The calibrations in the previous steps are used to choose this orientation.

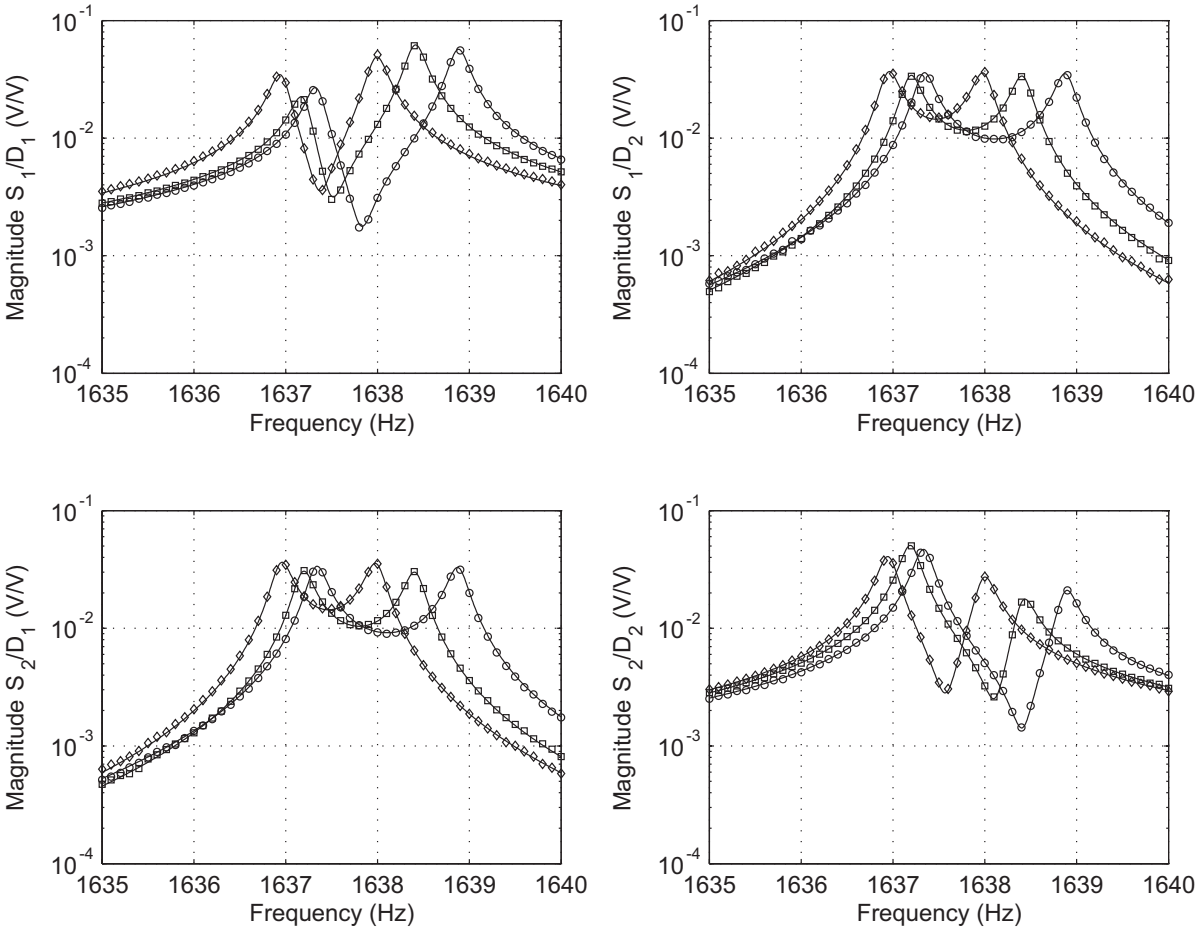

Figure 16: Frequency responses from steps 1 and 2 of the algorithm with their corresponding fit. '○' represents the empirical response from the unperturbed case, '□' represents the response when magnets are added only to spoke 4, and '◇' represents when magnets are added to spoke 4 and spoke 1. The solid traces represent the frequency responses of the model that was fit to the three data sets. The model associated with this fit is used to determine the number of magnets that are needed on each spoke to achieve a tuned state. The frequency response after the tuning magnets are added can be seen in Fig. 17.

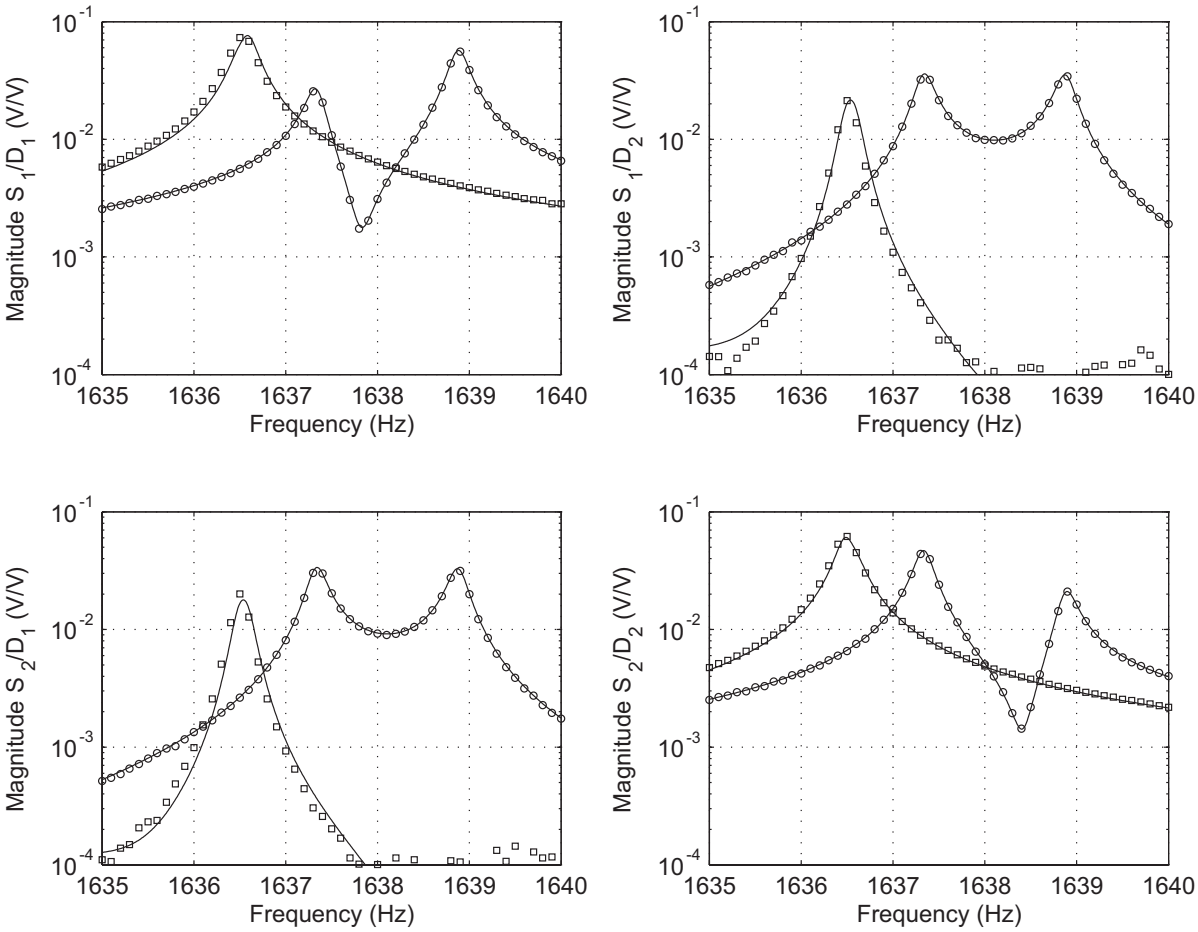

Figure 17: The empirical frequency response of the unperturbed resonator is again represented by '○', and exhibits a split of 1.52 Hz. Using the model of the data in Fig. 16, weightings of 3.2 magnets on spoke 1 and 7.2 magnets on spoke 4 are predicted to give a tuned state. '□' represents the empirical frequency response when 3 magnets are on spoke 1 and 7 magnets are on spoke 4. The solid line corresponding to this data is the predicted response using the model. The final split is 0.08 Hz.

$\{0, 15, \ldots, 75\}$ degrees from the D_1 axes for the initial arrangement. The results are shown in Table 1. The spoke $\#'s$ referred to in the table correspond to those in Fig. 15. The number of magnets placed on each spoke after the first three steps, including those used for calibration, are shown in fifth and sixth column[5] while the seventh column displays the resulting frequency split after these magnets are added. In each case the split is significantly reduced at this point, but in some cases an additional magnet on one spoke could further reduce the split. Ideally the correct amount of mass could be placed at the new location of the anti-node of the high frequency node to completely eliminate the split. We are, however, constrained to placement of mass only at the spokes, and can only add quantized amounts of mass. Thus, as a final fine tuning step, we add one additional magnet to the spoke closest to the new anti-node of the high frequency node if the split is larger than some threshold. The threshold is a function the amount a single magnet reduces the split, which, in the case of the Macro DRG, is at most 0.20 Hz. Utilizing what was learned from the experiment described in Fig 12, a magnet that is added when the split is smaller than 0.10 Hz is guaranteed to increase the split. Thus 0.10 Hz is chosen as this threshold.

The last two columns of Table 1 display the spoke on which the additional magnet is placed as well as the final frequency split. In all but one case the final frequency split is below the threshold.[6] The largest tuning mass perturbation was seventeen magnets total. This altered the mass of the Macro DRG resonator by 0.07% tuning a 0.14% frequency split.

[5]Unlike the example in the previous paragraph, only one magnet is used to calibrate each spoke for each case. This reduces the possibility of placing more magnets than necessary on a spoke. In the case displayed on the fifth row, however, the approximated position of the anti-node of the high frequency mode was close enough to spoke 1 that the optimization code called for nine magnets on spoke 1 and zero on spoke 2 total. Since one magnet had already been placed on spoke 2, an additional magnet was placed on spoke 4, which canceled out the effect of the calibration while still treating the perturbations as 'irreversible'. Thus the distribution of magnets after the first three steps is nine magnets on spoke 1, one on spoke 2 and one on spoke 4.

[6]In this one case the position of the anti-node of the high frequency mode after the first three steps was far enough away from the fine tuning spoke that the additional magnet did not reduce the split. A more complex threshold could easily derived for cases like this, but have been ignored here for simplicity.

Large Magnet Placement (degrees)	Initial Frequency split (Hz)	First Spoke (spoke #)	Second Spoke (spoke #)	Perturbation for first spoke (# of magnets)	Perturbation for second spoke (# of magnets)	Frequency Split (Hz)	Final Tuning Spoke (spoke #)	Final Frequency Split (Hz)
none	1.52	4	1	7	3	0.08	na	0.08
0	1.64	2	1	6	5	0.12	2	0.08
15	0.81	1	2	4	2	0.10	4	0.08
30	1.26	1	4	6	1	0.10	1	0.1
45	1.78	1	2	9	0	0.12	4	0.12
60	2.24	1	2	11	5	0.13	4	0.08
75	2.17	1	2	8	8	0.03	na	0.03

Table 1: Tuning results using the spokes algorithm with various initial mass distributions.

5 Conclusions

A mass matrix perturbation approach for tuning two modes to degeneracy in an axisymmetric resonator has been developed and experimentally verified on a large scale replica of a disk resonator gyro. The approach essentially identifies the perturbations to the nominal resonator mass matrix created by the addition (or removal) of a quantized amount of mass at several judiciously chosen locations on the resonator. The mass matrix perturbations are then used to estimate the total mass addition required at each location to render degenerate the modal frequencies of the two modes of interest. In practice, however, it is only necessary to reduce the frequency split to a prescribed level. For vibratory gyroscopes, the modal frequency split is directly related to the signal-to-noise ratio (SNR) of the angular rate signal, with larger splits reducing the SNR. A rule of thumb for these sensors is that the modal frequency split must be less than the bandwidth of each mode in order to maximize the SNR. In the present study the bandwidths of each mode are approximately 0.12 Hz so the stopping criteria of a 0.1 Hz split is justified. Since the allowable frequency split is reduced in proportion to the reduction in bandwidth of the modes, requirements can be developed for any proposed mass deposition/removal scheme. The quantized nature of the mass perturbation in the present study limits the change in frequency split to about 0.2 Hz per mass quanta, which is again compatible with the stopping criteria derived from the resonator bandwidth. One can anticipate significant engineering challenges in developing the fabrication machinery for mass

addition/removal on resonators with high quality factors.

Another promising direction to which the paper's model fitting tools can be applied is the problem of isolating selected resonator modes from linear acceleration of the resonator "stem." This problem is motivated by vibratory gyroscope applications in which the modes that are exploited for angular rate detection are, ideally, not coupled to linear acceleration of the sensor case. Coupling is always present in physical devices and produces spurious angular rate measurements when the sensor is subjected to vibration. It is desirable to reduce the coupling to linear acceleration and this can also be accomplished by the judicious removal or addition of mass at certain points on the resonator.

References

[1] Lynch, D.D., "Hemispherical Resonator Gyro," in Ragan, R.R. (ed.) "Inertial technology for the future," IEEE Trans. on Aerospace and Electronic Systems, AES-20, 4, pp. 414-444, 1984.

[2] Gripton, A. "The application and future development of a MEMS SiVSG for commercial and military inertial products" IEEE Position Location and Navigation Symposium, pp. 2835, April 2002.

[3] D.D. Lynch, "Coriolis Vibratory Gyros", Symposium Gyro Technology, Stuttgart Germany, September 1998.

[4] Adams, S.G., Bertsch, F.M., Shaw, K.A., and MacDonald, N.C., "Independent Tuning of Linear and Nonlinear Stiffness Coefficients," IEEE J. Microelectromechanical Systems, Vol. 7, No. 2, pp. 172-180, 1998.

[5] Ayazi, F., and Najafi, K., "A HARPS Polysilicon Vibrating Ring Gyroscope," IEEE J. Microelectromechanical Systems, Vol. 10, No. 2, pp. 169-179, 2001.

[6] Kim, D-J., and M'Closkey, R.T., "A systematic method for tuning the dynamics of electrostatically actuated vibratory gyros," IEEE Trans. Control System Technology, Vol. 14, No. 1, pp. 69-81, 2006.

[7] T. Charnley and R. Perrin "Perturbation studies with a thin circular ring." Acustica, Vol. 28, pp. 140-146, 1973.

[8] D. Allaei, W. Soedel and T. Y. Yang, "Natural frequencies of rings that depart from perfect axial symmetry." Journal of Sound and Vibration, Vol. 111, pp. 9-27, 1986.

[9] C. H. J. Fox . "A simple theory for the analysis and correction of frequency splitting in slightly imperfect rings" Journal of Sound and Vibration, Vol 142, pp. 227-243, 1990

[10] Gallacher, B. J., "Multi-modal tuning of a ring gyroscope using laser ablation" Proc. Inst. Mech. Eng. C.,Vol. 217, pp. 557-76, 2000.

[11] C.P. Fell, "Method for matching vibration mode frequencies on a vibrating structure" US Pat. 5739410, 1996.

[12] Abdelmoneum, M.A, Demirci, M.M., Lin, Y-W., and Nguyen, C.T., "Location-Dependent Frequency Tuning of Vibrating Micromechanical Resonators Via Laser Trimming," 2004 IEEE Int. Ultrasonics, Ferroelectrics, and Frequency Control Symp., pp. 272-279, 2004.

[13] Nayfeh, A. H., Younis, M. I., "A new approach to the modeling and simulation of flexible microstructures under the effect of squeeze-film damping," Journal of Micromechanics and Microengineering, Vol. 14, pp. 170-181, 2004.

[14] Sanathanan, C.K. and J. Koerner. "Transfer function synthesis as a ratio of two complex polynomials," IEEE Trans. on Automatic Control, AC–8, pp. 56-58, 1963.

[15] Zhbanov, Yu. K., and Zhuravlev, V. F., "On the Balancing of a Hemispherical Resonator Gyro," Mech. Solids, Vol. 33, No. 4, pp. 2-13, 1998.

[16] Enderling, S., Hedley, J., Jiang, L., Cheung, R., Zorman, C., Mehregany, M., and Walton, A., “Characterization of frequency using focused ion beam platinum deposition,” J. Micromech. Microeng., Vol. 7, pp. 213-219, 2007.

List of Figure Captions

- Figure 1: **Left:** Photograph of the resonant structure of the Boeing Silicon Disk Resonator Gyroscope (SiDRG). The n=2 Coriolis-coupled mode of the resonator is generally utilized for rate detection. **Right:** The SiDRG frequency response using embedded drive and sense electrodes within a narrow, 100 Hz band encompassing the fundamental Coriolis modes. Though the frequency split is small in a relative senseless than 0.3%the sensor effectively has no mechanical gain in this state.

- Figure 2: **Left:** Illustration of an n=2 Coriolis-coupled mode in a perfectly axisymmetric ring. This mode appears in a degenerate pair, meaning it can occur with any angular position relative to the axis of symmetry. Middle: When slight mass asymmetries exist, the modes manifest themselves in two fixed angular orientations, 45 degrees apart. These modes have two slightly different frequencies and cause the detuning seen in Fig. 1. **Right:** When the correct amount of mass is added to the anti-node of the high frequency mode (the target for tuning on the asymmetric detuned ring), a tuned state can be reached. Even though the mass distribution is asymmetric, the important properties of the ideal ring are recovered.

- Figure 3: **Left:** Photograph of the Macro DRG. The two electromagnetic actuators are labeled D_1 and D_2, and the two capacitive pick-offs, that detect radial deflection of the resonator, are labeled S_1 and S_2. Small NdFeB magnets are added to create a reversible perturbations of the mass distribution of the resonator. **Top Right:** Diagram of the electromagnetic actuator. **Bottom Right:** Diagram of the capacitive sense pick-off. This design was used to minimize electromagnetic coupling to the transimpedance amplifier.

- Figure 4: Block diagram of test setup. The filtered drive and sense signals are denoted D_i and S_i, i = 1,2, respectively. Frequency response data is used to construct a two-input/two-outputmodel of the Macro DRG dynamics. The dotted path represents an alternative setup that is used to calibrate gaps between the pick-offs and the resonator.

- Figure 5: **Left:** The S_1/D_1 channel of the empirical wideband frequency response of the Macro DRG showing several resonator modes. At this scale there appears to be no split between the n=2 modes (near 1.6 kHz). **Right:** The narrowband dynamics of all four channels in a neighborhood of the fundamental Coriolis-coupled modes. The data points are represented by '$\circ$ while the trace through the points is a model that was fit using the process described later in this paper. Just as in the SiDRG response, the Coriolis-coupled modes of the Macro DRG have a small frequency split despite the fact that the steel resonator is highly symmetric.

- Figure 6: **Left:** Orientation of Δ_1 perturbation. **Right:** Orientation of Δ_2 perturbation. Masses are added at four points in each case to achieve the most even possible mass loading. These are the perturbations corresponding to '$\square$' and '$\diamondsuit$' in Figs. 7 and 8.

- Figure 7: The two-input/two-output empirical and model frequency response magnitudes used to test the model fitting algorithm. The empirical data for the test with no perturbation is represented by '$\circ$' and the data resulting from the Δ_1 and Δ_2 perturbations (shown in Fig. 6) are represented by '$\square$' and '$\diamondsuit$' respectively. The model fits given by $(R_0 + j\omega R_1)\left(-(M_0 + \Delta_k)\omega^2 + K + j\omega C\right)^{-1}$ of the three data sets are the solid traces. Thus, the change in the frequency response due to the addition of magnets is successfully modeled as a change to only the mass matrix.

- Figure 8: The two-input/two-output empirical and model frequency response phase plots corresponding to the magnitude plots in Fig. 7.

- Figure 9: Empirical frequency response of Macro DRG with double the mass perturbation at the Δ_1 perturbation locations ('$\circ$') compared to the frequency response predicted by the model $(R_0 + j\omega R_1)\left(-(M_0 + 2\Delta_1)\omega^2 + K + j\omega C\right)^{-1}$ (solid trace).

- Figure 10: Empirical frequency response of Macro DRG with the mass perturbations in both the Δ_1 and Δ_2 perturbation locations ('$\circ$') compared to the frequency response predicted by

the model $(R_0 + j\omega R_1)\left(-(M_0 + \Delta_1 + \Delta_2)\omega^2 + K + j\omega C\right)^{-1}$ (solid trace).

- Figure 11: **Left:** Illustration of the testing setup used to determine the radial deflection of the outermost ring of the Macro DRG resonator. The driving electromagnet and the resonator are fixed on the rotational stage so that the deflection can be measured at 2 degree increments. **Right:** Plot of the radial deflection as a function of angular position. The dots represent the experimental data, while the dotted line is a sine wave fit. The large deviations from the sine wave are most likely caused by the additional stiffness provided by the spokes. One proposed tuning method involves adding mass directly to the resonator at the location corresponding to the anti-node of the experimental data. This is the method that has been used in the past to tune other ring shaped devices.

- Figure 12: **Left:** The five traces represent five experimental attempts to tune the Macro DRG by placing magnets at only one angular location, using locations of 72, 74, 76, 78 and 80 degrees. Data was taken when 0, 4, 6, 7, 8, 9 and 10 magnets were added for each case. The frequency splits are determined from the models that are fit to the individual experimentally determined frequency responses. In each case the split is at first reduced but at some point further addition of mass increases the split. It appears that the smallest split would be achieved near a location of 77 degrees. It is interesting to note that if the placement is as little as 3 degrees away from this location, the minimum split increases to nearly 0.4 Hz. **Right:** The data taken when tuning is attempted at 76 degrees is replicated as '$\circ$' in this plot. The solid line fit is done by fitting the empirical data from the first two points to a set $\{M_0, \Delta, C, K, R_0, R_1\}$ and using $\overline{\lambda}_{M_0+\frac{\alpha}{4}\Delta,K}$ and $\underline{\lambda}_{M_0+\frac{\alpha}{4}\Delta,K}$ to determine the split for any number of magnets (where α is the number of masses added). This is a good test of the predictive relevance of the model, but also shows how much the minimum achievable split is increased by using a quantized amount of mass.

- Figure 13: **Left:** Mass matrix perturbation, $\overline{\Delta}$, as a function of the counter-clockwise angle from the D_1 axes, θ, found by fitting the model to nine empirical frequency response data

sets. The upper diagonal term is denoted by '$\diamond$', the lower diagonal by '$\circ$', and the off diagonal term by '$\square$'. **Right:** Illustration of the eight placements of the magnet in the tests. When the experiment is repeated with different gap widths for the actuators and sensors, and different initial magnet distributions, the functional relationship varied only slightly. The absolute magnitudes are not important because the model parameter set is scaled by the $M_0 > I$ constraint in (6). The relative magnitudes, however, are at the very least interesting. The solid black magnet in the right hand picture illustrates the perturbation that corresponds to the data points that are solid black in the left-hand figure.

- Figure 14: Illustration of the assumed mode shape of the ring using $u = Acos\left(2\left(\theta - \Phi\right)\right)$, where Φ indicates the location of the anti-nodes of the mode shape, and u is the radial displacement of the mode shape as a function of the angle θ. We will use this notation to approximate the mode shape of the n=2 Coriolis-coupled mode of the Macro DRG.

- Figure 15: **Left:** Illustration of the identified spokes for mass loading for the example in the text. The gray axes represent the approximated anti-nodal axes of the unperturbed Macro DRG. The small white circles represent where the two magnets may be placed to calibrate the spoke 1, and the two black circles represent where two more may be added to calibrate spoke 4. **Right:** The final orientation of the magnets that successfully tunes the Macro DRG so that the anti-nodal axes are "trapped" between the tuning spokes. The calibrations in the previous steps are used to choose this orientation.

- Figure 16: Frequency responses from steps 1 and 2 of the algorithm with their corresponding fit. '$\circ$' represents the empirical response from the unperturbed case, '$\square$' represents the response when magnets are added only to spoke 4, and '$\diamond$' represents when magnets are added to spoke 4 and spoke 1. The solid traces represent the frequency responses of the model that was fit to the three data sets. The model associated with this fit is used to determine the number of magnets that are needed on each spoke to achieve a tuned state. The frequency response after the tuning magnets are added can be seen in Fig. 17.

- Figure 17: The empirical frequency response of the unperturbed resonator is again represented by '○', and exhibits a split of 1.52 Hz. Using the model of the data in Fig. 16, weightings of 3.2 magnets on spoke 1 and 7.2 magnets on spoke 4 are predicted to give a tuned state. '□' represents the empirical frequency response when 3 magnets are on spoke 1 and 7 magnets are on spoke 4. The solid line corresponding to this data is the predicted response using the model. The final split is 0.08 Hz.

List of Table Captions

- Table 1: Tuning results using the spokes algorithm with various initial mass distributions.